Insight into adsorption mechanism of cationic dye onto biosorbents derived from agricultural wastes

Hai Nguyen Tran[a,b*], Sheng-Jie You[a*], Tien Vinh Nguyen[c], and Huan-Ping Chao[a,*]

[a]Department of Environmental Engineering, Chung Yuan Christian University, Chungli 320, Taiwan

[b]Department of Civil Engineering, Chung Yuan Christian University, Chungli 320, Taiwan

[c]Faculty of Engineering and IT, University of Technology, Sydney (UTS), PO Box 123, Broadway, Sydney, Australia

Abstract

This study investigated the phenomenon and mechanism of adsorption of methylene green 5 (MG5) on three pristine biosorbents: golden shower pod (GS), coconut shell (CC), and orange peel (OP). The results showed that the biosorbents possessed low specific surface areas, but abundant functional groups. Adsorption was strongly affected by the solution's pH and ionic strength. As revealed in the kinetic study, equilibrium was rapidly established, requiring low activation energies; a removal rate of 30%–87% was achieved within 1 min. The maximum Langmuir adsorption capacities at 30 °C exhibited the following order: GS (106 mg/g) > OP (92 mg/g) > CC (59 mg/g). Thermodynamic experiments suggested that the adsorption occurred spontaneously ($-\Delta G°$) and exothermically ($-\Delta H°$). The primary adsorption mechanisms involved electrostatic attraction, hydrogen bonding formations, and n-π interaction. Thermogravimetric analysis revealed that three biopolymer components (i.e., hemicellulose, cellulose, and lignin) played controlling roles in the adsorption process. Thus, these three agricultural residues can be considered potential low-cost adsorbents for efficient dye adsorption applications.

Keywords: Biosorbent; cationic dye; adsorption mechanism; biopolymer; agricultural waste

* Corresponding authors:

H.-N. Tran (trannguyenhai2512@gmail.com), S.-J. You (sjyou@cycu.edu.tw), and H.-P. Chao (hpchao@cycu.edu.tw)

1. Introduction

The presence of dyes and pigments in water bodies is enormously concerning for public health. A variety of synthetic dyes are used in many industries, including leather, textile, paper, rubber, dyestuff, cosmetics, plastics, pharmaceutical, printing, food, paint, pigment, petroleum, pesticide and wood-preserving chemical industries. Notably, over 100,000 known commercial dyes exist, and of the approximately 700,000 tons of dye produced each year, 10,000 tons are subsequently discharged into wastewater streams (Raval et al., 2016). The uncontrolled and untreated discharge of abundant colored wastewater into the water environment has attracted substantial attention because dyes' toxic, carcinogenic, mutagenic, and allergenic properties adversely affect aquatic organisms and human health.

Adsorption technology is considered the most economically favorable technique to remove dyes among those available (i.e., membrane separation, oxidation, and irradiation) because of its high removal efficiency, low operation cost, and ability to separate a wide range of contaminants from industrial effluents. Various biosorbents derived from agricultural and industrial wastes have been efficiently applied to remove different types of dyes in the literature, such as acid, cationic, dispersive, direct, reactive, solvent, sulfur, and vat dyes (Annadurai et al., 2002; Gupta and Suhas, 2009; Contreras et al., 2012; Witek-Krowiak, 2013; Wang et al., 2014; Oladipo and Gazi, 2015; Roosta et al., 2015; Sadaf et al., 2015; Jeyagowri and Yamuna, 2016; Tahir et al., 2017). Although the removal efficiencies of biosorbents are lower than that of activated carbon, the industrial-scale utilization of these materials is economically attractive (Contreras et al., 2012).

Natural lignocellulosic biomasses from agricultural residues can be regarded as low-cost and renewable materials for the decolorization of wastewater effluents from the textile industry because of the presence of biopolymers, such as polysaccharides, lignin, hemicelluloses, and

cellulose. These biopolymers include abundant oxygen-containing functional groups and are potentially useful for the uptake of various contaminants from aqueous solutions. Methylene green 5 (MG5) is a cationic phenothiazine dye and heterocyclic aromatic chemical compound that can be considered as a nitro derivative of methylene blue. In addition, MG5—commonly used in various industries—shows considerable solubility in both polar organic media and water. However, the factors contributing to the adsorption of MG5 on agricultural residues-derived biopolymers have not been reported previously. In addition, the adsorption mechanisms of MG5 have not been thoroughly described in the literature. Knowledge of these adsorption mechanisms is criterial for determining the amounts of MG5 adsorbed on different biosorbents.

In this study, three biosorbents (i.e., golden shower pod [GS], coconut shell [CS], and orange peel [OP]) were used to investigate the uptake process of MG5 from an aqueous solution. The biosorbents were selected based on their popularity and different properties, especially the difference about the quantity of their biopolymer components (i.e., hemicellulose, cellulose, and lignin). The batch adsorption experiments were performed under different operation conditions (i.e., solution pH, ionic strength, contact time, initial concentration, temperature, and desorption agent) to determine their effects on the adsorption process. The important contributions of the tested biopolymers toward the total adsorption of MG5 were examined thoroughly by conducting detailed comparisons of the changes in the biosorbents' properties after adsorption using various techniques (i.e., thermogravimetric analysis [TGA], Fourier transform infrared [FT-IR] spectroscopy, and Boehm titration).

2. Materials and methods

2.1. Biosorbent preparation

The GS, CC, and OP were obtained from a local market in Taiwan. The collected samples were first washed with tap water at least three times and then with deionized distilled water to remove water-soluble impurities and surface-adhered particles. Then, they were placed in an oven at 105 °C for 48 h to remove excess water and moisture. The dried samples were ground and sieved to obtain the desired particle sizes (0.106–0.250 mm). The samples were stored in tightly closed brown glass bottles and used as potential biosorbents without any further treatment.

2.2. Biosorbent analysis

The biosorbent samples were degassed at 110 °C for 24 h in a vacuum oven before the measurements. The textural properties were measured by collecting nitrogen adsorption–desorption isotherms (Micromeritics ASAP 2020 sorptometer) at 77 K. The morphology of the adsorbents was determined using scanning electron microscopy (SEM; Hitachi S-4800, Japan) with an accelerating voltage of 3 kV. Before observation, the samples were coated with gold in E-1010 Ion sputter. The thermal stability was measured by TGA (DuPont TA Q50, USA) under an air atmosphere. The experiment was conducted from room temperature to 900 °C with a heating rate of 10 °C/min. Proximate analysis was performed by following an international standard procedure (ASTM).

The superficial chemistry of the biosorbent was elucidated using three techniques. Firstly, the functional groups present on the adsorbent surface were detected using FT-IR (FT/IR-6600 JASCO). The spectra were scanned from 4,000 to 650 cm^{-1}. Secondly, the pH values of the biosorbents at the point of zero charge (pH_{PZC}) were determined using "the drift method". Recently, Tran and coworkers (2017b) investigated the effects of operation conditions on the pH_{PZC} of

commercial activated-charcoal using "the drift method". The results demonstrated that the point of zero charge (9.81± 0.07) of charcoal was insignificantly dependent on the operation conditions (i.e., CO_2, solid/liquid ratio, electrolyte type, electrolyte concentration, and contact time). Thirdly, the quantities of acidic groups and basic sites on the adsorbent surface were determined through Boehm titration, following the standardized protocol proposed by Goertzen and coworkers (2010). The numbers of moles of adsorbent surface functionalities were determined from the equations reported in our recent publication (Tran et al., 2017e).

2.3. Dye adsorption study

2.3.1 Batch adsorption experiment

All of the MG5 solutions were serially diluted from an MG5 stock solution (1,000 mg/L). The stock solution was prepared by dissolving a given amount of MG5 in deionized distilled water. All chemicals used in this study were of analytical grade.

The effect of the pH on the dye adsorption capacity was measured by mixing 25-mL solutions containing 300-mg/L MG5 with 0.1 g of each biosorbent using solutions with various pH values. The initial pH value was adjusted from 2.0 to 10.0 ± 0.2 by adding 1-M NaOH or 1-M HCl. Similarly, the influence of the ionic strength was examined by varying the NaCl concentration from 0 to 0.5 M. The kinetic adsorption study was conducted using a series of 100-mL Erlenmeyer flasks containing 50 mL of MG5 solution at 30 °C and 50 °C. Adsorption isotherms were collected using MG5 concentrations ranging from approximately 100 to 1,000 mg/L at different temperatures. The thermodynamic parameters were estimated at three different temperatures for various MG5 concentrations (approximately 100–1,000 mg/L). The MG5-biosorbent mixtures were shaken using an orbital-shaking incubator (S300R-Firstek) at 150 rpm.

After predetermined intervals, the mixtures were separated using glass fiber filters. The MG5-laden biosorbent was rinsed with deionized distilled water, dried, and stored for further experiments (i.e., FT-IR, TGA, and desorption). The MG5 concentration in solution was determined using ultraviolet-visible spectrophotometry (Genesys 10 UV-Vis; Thermo Scientific) at the wavelengths of maximum absorption (Fig. 1). The amount of MG5 uptake at equilibrium, q_e (mg/g), was calculated by the mass-balance equation.

$$q_e = \frac{(C_o - C_e)}{m_1} V_1 \quad (1)$$

where C_o (mg/L) and C_e (mg/L) are the initial and equilibrium MG5 concentrations, respectively; m_1 (g) is the mass of biosorbent used; and V_1 (L) is the volume of the MG5 solution. All batch adsorption experiments were undertaken at a constant solid/liquid ratio of approximately 4.0 g/L.

Figure 1

The adsorption reversibility was determined by desorption experiments. A given mass of MG5-loaded biosorbent (m_2) was desorbed using 0.025 L of various desorbing agents (V_2). The amount of MG5 remaining on the biosorbent was estimated by the following mass-balance relationship:

$$q_r = q_e - q_d = q_e - \frac{C_d}{m_2} V_2 \quad (2)$$

where q_r (mg/g) is the mass of MG5 that remained adsorbed at the end of the desorption study, C_d (mg/L) is the concentration of MG5 in the solution after desorption, and q_d (mg/g) is the mass of MG5 desorbed if the adsorption was reversible.

2.3.2. Statistical analysis

All experiments were conducted in triplicate, and the results are expressed as the mean ± standard deviation. Trial-and-error non-linear methods were performed using the Solver

add-in (Microsoft Excel) to compute the parameters of the isotherm and kinetic models. The coefficient of determination (R^2) of the non-linear optimization method was computed using Eq. 3. To identify the best-fit model for the adsorption process, the chi-square (χ^2) and non-linear R^2 values were determined (Tran, You et al. 2016a, Tran, You et al. 2017f, Tran, You et al. 2017d).

$$R^2 = 1 - \frac{\sum (q_{e,exp} - q_{e,cal})^2}{\sum (q_{e,exp} - q_{e,mean})^2} = \frac{\sum (q_{e,cal} - q_{e,mean})^2}{\sum (q_{e,cal} - q_{e,mean})^2 + \sum (q_{e,cal} - q_{e,exp})^2} \quad (3)$$

$$\chi^2 = \sum \frac{(q_{e,exp} - q_{e,cal})^2}{q_{e,cal}} \quad (4)$$

where $q_{e,exp}$ (mg/g) is the MG5 uptake at equilibrium obtained from Eq. 1, $q_{e,cal}$ (mg/g) is the MG5 uptake determined from the model after using the Solver add-in, and $q_{e,mean}$ (mg/g) is the mean value of $q_{e,exp}$.

3. Results and discussion

3.1. Biosorbent characteristics

The basic properties of the biosorbents are listed in Table 1. Clearly, the biosorbents have low specific surface areas and total pore volumes, in agreement with their rough and heterogeneous morphologies shown in Figure 2. In addition, the biosorbents possess non-uniform sizes and shapes (Figure 2).

Table 1

Figure 2

Figure 3 and Table 2 present qualitative information on the functional groups (chemical bonds) available on the surfaces of the biosorbents and their spectroscopic assignments, respectively. The spectra of the three biomass samples are typical of lignocellulose material. The

intense bands at approximately 3400 cm^{-1} are assigned to the (–OH) stretching vibrations of the hydroxyl groups in hemicellulose, cellulose, and lignin. The moderate peaks observed at roughly 2920 cm^{-1} are attributed to either asymmetric or symmetric C–H stretching vibrations of the methyl ($–CH_3–$) and methylene ($–CH_2–$) groups, as expected for hemicellulose, cellulose, and lignin (Köseoğlu and Akmil-Başar, 2015). The presence of a carbon-carbon triple bond (C≡C) in disubstituted alkynes is indicated by the peaks at approximately 2350 cm^{-1}. The presence of carboxylic and lactonic groups (C=O) is evidenced by the well-defined bands at roughly 1470 cm^{-1}. Similarly, the recognized bands at approximately 1620 cm^{-1} are ascribed to C=C double bonds in aromatic rings. The IR peaks near 1250 cm^{-1} are attributable to the C–O–C stretching of aryl-alkyl ether linkages in lignin (Yang et al., 2007). Notably, the characteristic peak of C–O–C in the spectrum of OP exhibited a very low intensity, indicating that the OP might contain less lignin compounds than the woody samples (i.e., GS and CC). Finally, the C–O stretching vibrations of cellulose structure are responsible for the sharp bands at approximately 1050 cm^{-1} (Mujtaba et al., 2016; Tran, You et al. 2017f).

Figure 3

Table 2

The pyrolytic characteristics of the examined biomass were determined using a thermogravimetric analyzer, and they are presented in Figure 4 and Table 3. For the MG5-unloaded biosorbent, four overlapping peaks corresponding to the maximum weight loss values are observed in the thermogravimetric curves, except for that of OP. The weight loss temperatures (T_{max}) were lower than 85 °C because of the vaporization of moisture, and the thermal decomposition peaks at T_{max} values of 237–299 °C, 327–341 °C, and 498–700 °C were attributed to the thermal

degradation of hemicellulose, cellulose, and lignin, respectively. These results are consistent with those of Yang and colleagues (2007). They noted that the pyrolysis of pure hemicellulose and cellulose occurred at 220–315 °C (T_{max} = 268 °C) and 315–400 °C (T_{max} = 335 °C), whereas pure lignin was more difficult to decompose (160–900 °C). The weight loss values of the three main components of the tested biomasses exhibited the following order: lignin (37.9%) > cellulose (30.1%) > hemicellulose (26.8%) for GS; lignin (33.2%) > hemicellulose (28.7%) > cellulose (23.5%) > for CC; and cellulose (32.4%) > lignin (27.9%) > hemicellulose (19.5%) for OP. The onset and endset values of the biosorbents, which were extrapolated based on the intersection of two tangent lines of the TGA curves, provide additional useful information regarding the thermal stability of these biomasses. The onset and endset of CC (244 and 641 °C) were higher than those of GS (244 and 605 °C) and OP (188 and 337 °C), respectively, indicating that GS is more thermally stable than the other tested biosorbents.

Figure 4

Table 3

3.2. Effects of pH and ionic strength

The surface charges of the biosorbents in solution were characterized by the point of zero charge (PZC). The PZC was defined as the pH value at which the net (external and internal) surface charges on an adsorbent are zero. Essentially, when the pH of a solution ($pH_{solution}$) exceeds the pH_{PZC}, the adsorbent's surface becomes negatively charged because of the deprotonation of oxygen-containing surface groups (i.e., –COOH and –OH), favoring the adsorption of cationic ions from the solution and vice versa. The pH_{PZC} values of the biosorbents were as follows: CC (pH_{PZC} = 6.5) > OP (5.3) > GS (3.8). Thus, the acidic oxygen-containing functional groups

exhibited the following order: GS (8.74 mmol/g) > OP (6.90 mmol/g) > CC (4.21 mmol/g) (Figure 5a and Table 1).

The pH dependence of MG5 adsorption is presented in Figure 5b. Clearly, the adsorption of MG5 by the biosorbent occurred when $pH_{solution} < pH_{PZC}$. Indeed, at a low pH (2.0), the biosorbents were still able to adsorb MG5 molecules, although at this pH, the excess H^+ ions present in the system showed strong competition with the cationic MG5 molecules for the active adsorption sites. Notably, this was not observed for CC. This result might indicate that mechanisms other than electrostatic attraction (i.e., hydrogen bonding or n-π interactions) exist. The dye-removal capacity is highly dependent on the pH_{PZC} of the biosorbent. The amount of dye adsorbed increased substantially as the solution pH increased and plateaued when $pH_{solution} > pH_{PZC}$ (Figure 5b). An analogous result was found in the literature (Ncibi et al., 2009).

Figure 5c shows the influence of the ionic strength on the MG5 uptake. Clearly, the adsorption capacities of the biosorbents were inhibited by the presence of univalent electrolyte in the solution. The magnitude of the effect of the NaCl concentration on q_e (mg/g) varies widely between adsorbents. For example, 0.05 M of Na^+ ions is sufficient to compete with MG5 ions for the binding sites on the surfaces of GS and CC, whereas for OP, a concentration of 0.1 M is needed. Therefore, the following conclusions can be drawn: (1) a screening effect (known as electrostatic screening) exists between the positively charged biosorbent surface and MG5 molecules, and (2) the electrostatic force plays a vital role in the adsorption mechanism.

Figure 5

3.3. Adsorption kinetics

The effect of the contact time on the uptake amount of MG5 at different temperatures is described in Figure 6. The dye-removal rate increased continuously during the initial 10 min of

contact; subsequently, the removal rate decreased slightly and plateaued after approximately 30 min for OP, 60 min for CC, and 120 min for GS. In addition, the amount of dye removed decreased at higher temperatures, suggesting that the adsorption process is favored at lower temperatures. The instantaneous adsorption phenomenon indicated that the biosorbents have strong affinities for the cationic dye molecules. The kinetics plays a significant role, facilitating scaling the process up to small reactor volumes to ensure efficiency and economy.

Figure 6

In this study, several kinetic models were applied to mathematically describe the intrinsic adsorption constants. The non-linearized forms of the pseudo-first-order (Lagergren, 1898) and pseudo-second-order (Blanchard et al., 1984) models are expressed in Eqs. 5–6. The Elovich model (Roginsky and Zeldovich, 1934) and intra-particle model (Weber and Morris, 1963) are presented in Eqs 7–8, respectively.

$$q_t = q_e(1-e^{-k_1 t}) \tag{5}$$

$$q_t = \frac{q_e^2 k_2 t}{1+k_2 q_e t} \tag{6}$$

$$q_t = \frac{1}{\beta}\ln(1+\alpha\beta t) \tag{7}$$

$$q_t = k_{ip}\sqrt{t} + C \tag{8}$$

where k_1 (1/min), k_2 (g/mg × min), α (mg/g × min), and k_{ip} (mg/g × min) are the rate constants of the pseudo-first-order, pseudo-second-order, Elovich, and intra-particle diffusion models, respectively; q_e and q_t are the amounts of MG5 uptake per mass of the biosorbent at equilibrium and any time t (min), respectively; β (mg/g) is the desorption constant during any one experiment; and C (mg/g)

247 is a constant describing the thickness of the boundary layer. Higher values of C correspond to a
248 greater effect on the limiting boundary layer.

249 The activation energy of the sorption process (*Ea*; kJ/mol) can be predicted using the
250 Arrhenius equation. Eq. 10 describes the activation energy estimated based on adsorption kinetics
251 experiments performed at two temperatures:

$$k = Ae^{-E_a / RT} \tag{9}$$

$$\ln k_{(323K)} - \ln k_{(303K)} = (\ln A - \frac{E_a}{RT_2}) - (\ln A - \frac{E_a}{RT_1}) \quad \Leftrightarrow \quad E_a = \frac{R \ln \frac{k_{(323K)}}{k_{(303K)}}}{\frac{1}{T_1} - \frac{1}{T_2}} \tag{10}$$

252 where $k_{(323K)}$ *and* $k_{(303K)}$ are the rate constants of the kinetic model at 323 K and 303 K,
253 respectively; *A* is the pre-exponential factor (i.e., the frequency factor); *R* is the universal gas
254 constant (8.314 kJ/mol × K); and *T* is the absolute temperature in Kelvin.

255 Table 4 lists the relative kinetic parameters for dye adsorption at two temperatures.
256 According to the coefficient of determination (R^2), and chi-square (χ^2), it can be concluded that the
257 experimental data of adsorption kinetics were adequately described by the Elovich model (R^2 =
258 0.955–0.994 and χ^2 = 0.089–8.681) than the others, such as the intra-particle diffusion model
259 (0.739–0.911 and 0.161–13.07), the pseudo-second-order model (0.475–0.963 and 1.514–9.165),
260 and the pseudo-first-order model (0.258–0.874 and 5.105–30.81), respectively. The better fit of
261 experimental data with the Elovich model suggested that the surfaces of biosorbent are a
262 heterogeneous system, which is in accordance with the observation of their morphology in Figure
263 2.
264

As demonstrated in Table 4, the adsorption rates (i.e., k_1, k_2, and α) of the biosorbents exhibited the following order: OP > CC > GS. This result is consistent with the order determined for the removal percentages of MG5 at 1 min and 5 min of contact: 87% and 93% (OP) > 71% and 78 % (CC) > 30% and 52 % (GS), respectively. Equilibrium was established rapidly because (1) the low activation energies (*Ea*) were required (Tran, You et al. 2017f), and (2) the adsorption process only occurred in two steps associated with transport processes (Figure 6). In addition, the negative values of *Ea* (from –62.23 to –3.52 kJ/mol) reflected the exothermic nature of the adsorption process, and the low values of this parameter confirmed that physical adsorption occurred via relatively weak attraction forces.

Notably, the rates (i.e., k_1, k_2, and α) of MG5 adsorption remarkably decreased with an increase in temperatures, confirming that the adsorption process occurred with a slower speed when the temperature of the solution increased.

Table 4

3.4. Adsorption isotherms

Although adsorption isotherms can contribute to elucidating adsorption mechanisms, it is less helpful in this regard than kinetics and thermodynamics. However, collecting adsorption isotherms is a useful strategy to both describe the relationship between the adsorbate concentration in the solution (liquid phase) and the adsorbent (solid phase) at a constant temperature and design adsorption systems. In this study, the Langmuir (Eq. 11), Freundlich (Eq. 12), and Dubinin-Radushkevich (Eqs. 13–15) models were employed to describe both the adsorptive behavior of

cationic dye on different biosorbents. To minimize the respective error functions, the non-linear optimization technique was employed to calculate the adsorption parameters using these models.

$$q_e = \frac{Q^0_{\max} K_L C_e}{1 + K_L C_e} \tag{11}$$

$$q_e = K_F C_e^n \tag{12}$$

$$q_e = q_{DR} e^{-K_{DR}\varepsilon^2} \tag{13}$$

$$\varepsilon = RT \ln\left(1 + \frac{1}{C_e}\right) \tag{14}$$

$$E = \frac{1}{\sqrt{2K_{DR}}} \tag{15}$$

where q_e and C_e are obtained from Eq. 1; Q^o_{max} (mg/g) is the maximum saturated monolayer adsorption capacity of the adsorbent; K_L (L/mg) is the Langmuir constant related to the affinity between the adsorbent and adsorbate; K_F [(mg/g)/(mg/L)^n] is the Freundlich constant, which characterizes the strength of adsorption; n (dimensionless; $0 < n < 1$) is a Freundlich intensity parameter that reflects the magnitude of the adsorption driving force or surface heterogeneity (the adsorption isotherm becomes linear for $n = 1$, favorable for $n < 1$, and unfavorable for $n > 1$; (Hai, 2017)); q_{RD} (mg/g) is the adsorption capacity; K_{RD} (mol^2/kJ^2) is a constant related to the sorption energy; ε is the Polanyi potential; and E (kJ/mol) is the mean adsorption energy.

Hall and colleagues (1966) stated that the essential characteristics of the Langmuir isotherm model can be expressed in terms of a dimensionless constant separation factor or equilibrium parameter R_L, which is defined as follows:

$$R_L = \frac{1}{1 + K_L C_o} \tag{16}$$

where R_L is a constant separation factor (dimensionless), K_L is a Langmuir equilibrium constant, and C_o is the initial MG5 concentration. The isotherm shape was used to predict whether the adsorption system was favorable ($0 < R_L < 1$), unfavorable ($R_L > 1$), linear ($R_L = 1$), or irreversible ($R_L = 0$).

The MG5 adsorption isotherms for the biosorbents at different operation temperatures are presented in Figure 7. Clearly, the region in which the experimental data relating to the adsorption equilibrium are located is the Langmuir region, which is characterized by saturation at high concentrations. The higher determination coefficient (R^2) and lower chi-square (χ^2) values of the Langmuir model relative to those of the Freundlich model supports this hypothesis (Table 5). Thus, the Langmuir model adequately described the equilibrium adsorption data.

According to the classification of adsorption isotherm shapes proposed by Giles and coworkers (1974), the isotherm shapes of GS and CC (Figure 7) were classified as H-type (high affinity); this type is characterized by extremely strong adsorption at low concentrations, followed by a pseudo-plateau. In contrast, the isotherm shape of OP could be classified as L-type (Langmuir); an initial concave region relative to the concentration axis characterizes this type. This result could support the assumption that the CC and GS samples would exhibit different adsorption mechanisms relative to the OP sample.

Figure 7

Table 5 lists the adsorption parameters obtained under the three temperatures tested. The maximum monolayer adsorption capacities for MG5 were ranked as follows: GS (106 mg/g) > OP (92 mg/g) > CC (59 mg/g). As shown in Figure 7, the adsorption efficiency is strongly affected by the operation temperature. The uptake amount of MG5 decreased as the temperature increased,

indicating that the dye-adsorption process is exothermic. The decrease in the adsorption capacity at higher temperatures is ascribed to the decrease of the adsorption energy *Ea* (Table 5). Furthermore, the *Ea* values of the OP sample (0.018–0.031 kJ/mol) were substantially lower than those of GS (0.18–0.87 kJ/mol) and CC (0.191–0.213 kJ/mol), demonstrating that GS and CC might possess different adsorption mechanisms than OP.

Table 5

3.5. Adsorption thermodynamics

Thermodynamic studies are an indispensable component of predicting adsorption mechanisms (e.g., physical and chemical). The thermodynamic parameters can be computed according to the laws of thermodynamics using the following equations:

$$\Delta G^o = -RT \ln K_C \tag{17}$$

ΔG^o, ΔH^o, and ΔS^o are related as follows:

$$\Delta G^o = \Delta H^0 - T\Delta S^0 \tag{18}$$

The well-known van't Hoff equation is obtained by substituting Eq. 17 into Eq. 18

$$\ln K_C = \frac{-\Delta H^o}{R} x \frac{1}{T} + \frac{\Delta S^o}{R} \tag{19}$$

The Gibbs energy change (ΔG^o) can be directly calculated from Eq. 17, whereas the enthalpy change (ΔH^o) and entropy change (ΔS^o) were determined from the slope and intercept, respectively, of a plot of $\ln K_C$ against 1/T (Eq. 19). The equilibrium constant (K_C) must be dimensionless. In this study, the K_C derived from the Langmuir constant (K_L) was employed to

calculate the thermodynamic parameters (ΔG^o, ΔH^o, and ΔS^o). Thus, K_C can be easily obtained as a dimensionless parameter by multiplying K_L by 10^6 (the solution density, assuming that the density of pure water is 1.0 g/mL) (Milonjić, 2009; Tran, You et al. 2016b; Tran, You et al. 2017d)

The thermodynamic parameters of the dye adsorption process are listed in Table 6. The negative values of $\Delta G°$ at all investigated temperatures suggest that the adsorption phenomenon occurred favorably and spontaneously. This conclusion is in good agreement with the hypotheses relating to the separation factor ($0 < R_L < 1$) and Freundlich exponent n described in Section 3.4. Meanwhile, the negative $\Delta H°$ reflects the exothermic nature of the adsorption process, which was demonstrated by a decrease in the adsorption capacity (Figures 6–7) and the equilibrium constant (Table 6) at higher temperatures. The $-\Delta H°$ values also imply that energy is released as heat to the surroundings via physisorption, chemisorption, or a mixture of both processes (comprehensive adsorption). However, the low $\Delta H°$ magnitudes (from –28.33 to –4.15 kJ/mol) indicate that MG5 is removed via physisorption (Tran et al., 2016b). $\Delta S°$ exhibits the opposite trend relative to those of $-\Delta H°$ and $\Delta G°$ for the three biosorbents. The dye adsorption onto GS and CC is increasingly random ($\Delta S° > 0$), whereas that onto OP becomes less random ($\Delta S° < 0$). This difference involves the sign of the entropy change and may indicate that these materials exhibit different adsorption mechanisms.

Table 6

3.6. Adsorption reversibility

To some extent, adsorption mechanisms can be elucidated based on desorption studies. The adsorption reversibility was investigated using various desorbing agents, such as deionized water

(pH 2.0), 0.1-M HCl, methanol, and 0.1-M NaCl. If the dye adsorbed onto the adsorbents surface is easily desorbed by NaCl or HCl, the adsorption mechanism must involve electrostatic attraction between the negatively changed groups (i.e., $–COO^–$) on the surface of the biosorbent and the cationic MG5 molecules. In contrast, the desorption of dye by methanol might correspond to other types of interactions (i.e., hydrogen bonding or n-π interactions). Based on Figure 8, which presents the percentage values of MG5 desorption, the primary mechanisms for MG5 adsorption are electrostatic interactions (> 16% for GS, 28% for CC, and > 60% for OP) and other interactions involving the oxygen-containing functional groups on the biosorbent surface (approximately 76% for GS, 62% for CC, and 34% for OP). Cation exchange could play a minor role in the adsorption of the dye onto the adsorbents (below 10%). Based on the isotherm shapes and the results of the kinetic study, the effects of the pH and ionic strength, the adsorption energy, thermodynamics, and the desorption study, GS and CC likely have similar adsorption mechanisms.

Figure 8

3.7. Possible adsorption mechanisms

Generally, the possible mechanisms of cationic dye adsorption onto biosorbents are as follows: (1) electrostatic attraction, (2) hydrogen bonding, and (3) n-π interactions (Tran et al., 2017f). Notably, the specific surface areas of the analyzed biosorbents exhibited the following order: GS (5.72 m^2/g) > CC (3.16 m^2/g) > OP (2.08 m^2/g); in contrast, the maximum adsorption capacities were as follows: GS (106 mg/g) > OP (92 mg/g) > CC (59 mg/g). Therefore, the specific surface area is relatively less important for the adsorption capacities of these three biosorbents.

Weak electrostatic attractions can occur between the negatively charged sites on the surface of OP and the cationic MG5 molecules in the solution. Clearly, when $pH_{solution} > pH_{PZC}$, the oxygen-containing functional groups (i.e., carboxylic and phenolic groups) become ionized, and

thus, the pH of the solution decreases after adsorption (Figure 5d). The p*K*a values of the carboxylic (2.0–4.0) and phenolic (8.0–9.0) groups also play a role in explaining the biosorbents' surface charges. Both the carboxylic and phenolic groups can undergo dissociation, and can become predominantly negatively charged when the solution pH exceeds their p*K*a values. The pH of the solution used in this study was nearly 7.0, and at this pH value, the (–COOH) carboxylic groups dissociate, forming negatively charged carboxylate ($–COO^-$) groups. Thus, the carboxylic groups directly account for the binding of MG5 onto the biosorbent surface (Figure 9a). This finding is in agreement with the observed effects of the pH and ionic strength and the pH values after adsorption and desorption.

Hydrogen bonding interactions can occur (1) between the surface hydrogens of the hydroxyl groups (H-donors) on the adsorbent's surface and the appropriate atoms (i.e., nitrogen and oxygen; H-acceptors) of MG5 (this phenomenon is also known as dipole−dipole hydrogen bonding; Figure 9b) and (2) between the hydroxyl groups on the AC's surface and the aromatic rings of MG5 (this phenomenon is also known as Yoshida hydrogen bonding; Figure 9c). The FT-IR results demonstrated that the –OH groups at approximately 3400 cm^{-1} dramatically decreased in intensity (Figure 3) and shifted toward slightly higher wavenumbers (Table 2), confirming the existence of both dipole−dipole and Yoshida hydrogen bonding interactions (Blackburn, 2004). However, OP exhibited the opposite behavior, showing an insignificant decrease in the intensity of the peak at 3400 cm^{-1}. Therefore, the hydrogen bonding interactions contribute little to the adsorption mechanisms of OP.

n-π interactions (or n-π electron donor-acceptor interactions) were originally proposed by Mattson and colleagues (1969). In these interactions, the carbonyl oxygens on the surface of the adsorbent act as electron donors, and the aromatic rings of MG5 act as electron acceptors (Figure

9d). The FT-IR spectra revealed that the C=O and C–O peaks shifted and decreased in intensity after MG5 adsorption (Figure 3 and Table 2). The shifts of the C=O and C–O peaks after the adsorption of this aromatic species is consistent with previously reported results (Xing et al., 1994; Tran et al., 2017f; Tran et al., 2017g). As found for hydrogen bonding, n-π interactions did not constitute a major mechanism for adsorption on OP, as evidenced by the slight decreases in the intensities of the C=O and C–O peaks.

The changes in the TGA curves before and after MG5 adsorption provide additional information about the adsorption mechanisms. The onset and endset points of the three biosorbents shift toward higher values (Figure 4 and Table 3), confirming the successful adsorption of MG5 on the biosorbent surface. Moreover, derivative thermogravimetric analysis (DTG) data revealed that the magnitudes of the three components (i.e., hemicellulose, cellulose, and lignin) decreased remarkably after adsorption. Thus, these three components contribute to dye adsorption. However, the extent of their contributions may depend strongly on their amounts.

Assuming that the percentages of the dye desorbed by (1) HCl and NaCl reflected the electrostatic attraction and (2) methanol indicated the interactions of oxygen-containing functional groups, the contributions of these different adsorption mechanisms for the three adsorbents could be described as follows: hydrogen bonding and n-π interactions (76% and 62%) and electrostatic attraction (17% and 28%) for GS and CC, respectively; and electrostatic attraction (74%) and hydrogen bonding and n-π interactions (34%) for OP.

To identify the functional groups responsible for the adsorption, the dependence of the MG5-adsorption capacity on the surface chemistry of the biosorbents were determined by analyzing a plot of the Q^o_{max} from the Langmuir model (Table 5) versus the functional groups (Table 1). The results indicated that, based on the extremely high linear regression coefficient (R^2

= 0.996), the acidic groups were involved in the dye-adsorption process, unlike the basic groups (R^2 = 0.566). Among the acidic groups, the carboxylic groups played a more important role in the adsorption of MG5 (R^2 = 0.9803) compared to the phenolic (R^2 = 0.6116) and lactonic (R^2 = 0.4091) groups. Our recent study (Tran et al., 2017g) also demonstrated that the concentrations of total acid groups (i.e., carboxylic and phenolic) on the hydrochar's surface determined the selective adsorption order of the adsorbents: GSH > CCH > OPH.

The interactions responsible for the adsorption of MG5 molecules by the tested biosorbents are summarized in Figure 9.

Figure 9

3.8. Comparison

Because few studies have measured the removal of MG5 from solution by biosorbents, Table 7 compares the Q^o_{max} values determined in this study with previously reported Q^o_{max} values for various cationic dyes using different types of biosorbents. Clearly, the selective trend of the maximum adsorption capacity is inversely proportional to the molecular weight (M_w) of the dye. According to Table 7, GS, CC, and OP are attractive alternatives for the removal of cationic dyes from aqueous solutions.

Table 7

Furthermore, we also compared the S_{BET} and Q^o_{max} of MG5 adsorption onto the biosorbents in this study with those of the other adsorbents in the previous literature (Table 8). Theses adsorbents comprised hydrochar (Tran et al., 2017g), biochar (Tran et al., 2017c), non-spherical activated carbon (Shiau and Pan, 2005; Tran et al., 2017b; Tran et al., 2017f), spherical activated carbon (Huang et al., 2014; Tran et al., 2017a), silver nanoparticles-loaded activated carbon (Ag-NP-AC) and zinc oxide nanorods-loaded activated carbon (ZnONR-AC) (Ghaedi et al., 2014),

mesoporous zeolite (MCM-41) (Lee et al., 2007), glucose hydrochar modified with 1% triethylenetetramine (GH-TETA$_{1\%}$) and activated carbon modified with 1% triethylenetetramine (GAC1%) (Tran et al., 2017a), montmorillonite and activated clay (Shiau and Pan, 2005), titania nanotube (Lin et al., 2010). The difference on the Q^o_{max} values between these adsorbents might result from different primary adsorption mechanisms. For example, the MG5 adsorption mechanisms for adsorption onto biosorbent and hydrochar were mainly regarded as electrostatic attraction, while these for biochar and activated carbon were π–π interaction and pore filling. Furthermore, the differences in the adsorbent's characteristics (i.e., textural properties and surface chemistry) also caused the different the Q^o_{max} values.

Generally, in the same feedstock (i.e., golden shower pod as a typical example), the S_{BET} values followed activated carbon > biochar > hydrochar > biosorbent and the density of oxygen-contain functionalities followed biosorbent > hydrochar > activated carbon > biochar. In contrast, the Q^o_{max} values exhibited the following order: activated carbon > biosorbent > hydrochar > biochar. Therefore, to some extent, the density of oxygen-containing functionalities of an adsorbent played a more critical role than its BET specific surface area. A comprehensive comparison of the properties (i.e., textural, structural, morphological, physicochemical, crystal, thermally stable properties, and surface chemistry) of activated carbons prepared from different chemical activation methods and their precursors (i.e., biosorbent, hydrochar, and biochar) has been reported in detail in our recent study (Tran et al., 2017e).

Table 8

4. Conclusions

The adsorption process was strongly dependent on the pH of the dye solution and the presence of the electrolyte. The kinetic study confirmed that adsorption equilibrium was established rapidly with low activation energies (from –48.6 to –7.23 kJ/mol), and that, removal rates of 30%–87% and 52%–93% can be achieved within 1 min and 5 min of contact, respectively. The maximum monolayer adsorption capacities were ranked as follows: GS (106 mg/g) > OP (92 mg/g) > CC (59 mg/g). The thermodynamic study suggested that the dye adsorption occurred spontaneously ($-\Delta G°$) and exothermically ($-\Delta H°$). The primary adsorption mechanisms involved electrostatic interaction, hydrogen bonding formations, and n-π interaction. The carboxylic groups played a dominant role in the adsorption process, and the three biopolymer components (i.e., hemicellulose, cellulose, and lignin) contributed substantially. These three agricultural wastes could be low-cost, renewable candidates for efficient dye adsorption.

Acknowledgements

This current work was financially supported by Chung Yuan Christian University (CYCU) in Taiwan. The first author would like to thank CYCU for the Distinguished International Graduate Students (DIGS) scholarship to pursue his doctoral studies. The authors gratefully acknowledge the five anonymous reviewers for their invaluable insight and helpful suggestion to improve the quality and acceptability of the paper.

References

Annadurai, G., R.-S. Juang and D.-J. Lee (2002). Use of cellulose-based wastes for adsorption of dyes from aqueous solutions. Journal of Hazardous Materials, **92**(3), 263-274.

Blackburn, R. S. (2004). Natural Polysaccharides and Their Interactions with Dye Molecules: Applications in Effluent Treatment. Environmental Science & Technology, **38**(18), 4905-4909.

Blanchard, G., M. Maunaye and G. Martin (1984). Removal of heavy metals from waters by means of natural zeolites. Water Research, **18**(12), 1501-1507.

Contreras, E., L. Sepúlveda and C. Palma (2012). Valorization of Agroindustrial Wastes as Biosorbent for the Removal of Textile Dyes from Aqueous Solutions. International Journal of Chemical Engineering, **2012**, 9.

Ghaedi, M., H. Karimi and F. Yousefi (2014). Silver and zinc oxide nanostructures loaded on activated carbon as new adsorbents for removal of methylene green. Human & Experimental Toxicology, **33**(9), 956-967.

Giles, C. H., D. Smith and A. Huitson (1974). A general treatment and classification of the solute adsorption isotherm. I. Theoretical. Journal of Colloid and Interface Science, **47**(3), 755-765.

Goertzen, S. L., K. D. Thériault, A. M. Oickle, A. C. Tarasuk and H. A. Andreas (2010). Standardization of the Boehm titration. Part I. CO_2 expulsion and endpoint determination. Carbon, **48**(4), 1252-1261.

Gupta, V. K. and Suhas (2009). Application of low-cost adsorbents for dye removal – A review. Journal of Environmental Management, **90**(8), 2313-2342.

Hall, K. R., L. C. Eagleton, A. Acrivos and T. Vermeulen (1966). Pore- and Solid-Diffusion Kinetics in Fixed-Bed Adsorption under Constant-Pattern Conditions. Industrial & Engineering Chemistry Fundamentals, **5**(2), 212-223.

Hai, T. N. (2017). Comments on "Effect of Temperature on the Adsorption of Methylene Blue Dye onto Sulfuric Acid–Treated Orange Peel". Chemical Engineering Communications, **204**(1),134-139.

Huang, F.-C., C.-K. Lee, Y.-L. Han, W.-C. Chao and H.-P. Chao (2014). Preparation of activated carbon using micro-nano carbon spheres through chemical activation. Journal of the Taiwan Institute of Chemical Engineers, **45**(5), 2805-2812.

Jeyagowri, B. and R. T. Yamuna (2016). Potential efficacy of a mesoporous biosorbent Simarouba glauca seed shell powder for the removal of malachite green from aqueous solutions. Desalination and Water Treatment, **57**(24), 11326-11336.

Köseoğlu, E. and C. Akmil-Başar (2015). Preparation, structural evaluation and adsorptive properties of activated carbon from agricultural waste biomass. Advanced Powder Technology, **26**(3), 811-818.

Lagergren, S. (1898). About the theory of so-called adsorption of soluble substances. Kungliga Svenska Vetenskapsakademiens Handlingar, **24**(4), 1-39.

Lee, C.-K., S.-S. Liu, L.-C. Juang, C.-C. Wang, K.-S. Lin and M.-D. Lyu (2007). Application of MCM-41 for dyes removal from wastewater. Journal of Hazardous Materials, **147**(3), 997-1005.

Lin, K.-S., H.-W. Cheng, W.-R. Chen and C.-F. Wu (2010). Synthesis, characterization, and adsorption kinetics of titania nanotubes for basic dye wastewater treatment. Adsorption, **16**(1), 47-56.

Mattson, J. A., H. B. Mark, M. D. Malbin, W. J. Weber and J. C. Crittenden (1969). Surface chemistry of active carbon: Specific adsorption of phenols. Journal of Colloid and Interface Science, **31**(1), 116-130.

Milonjić, S. K. (2009). Comments on "removal of uranium (VI) from aqueous solution by adsorption of hematite", by X. Shuibo, Z. Chun, Z. Xinghuo, Y. Jing, Z. Xiaojian, W. Jingsong. Journal of Environmental Radioactivity, **100**(10), 921-922.

Mujtaba, M., I. Sargin and M. Kaya (2016). Determination of Bovine Serum Albumin Adsorption Capacity of Newly Obtained Cellulose extracted from Glycyrrhiza glabra (Licorice). Advances in Polymer Technology.

Ncibi, M. C., A. M. B. Hamissa, A. Fathallah, M. H. Kortas, T. Baklouti, B. Mahjoub and M. Seffen (2009). Biosorptive uptake of methylene blue using Mediterranean green alga Enteromorpha spp. Journal of Hazardous Materials, **170**(2–3), 1050-1055.

Oladipo, A. A. and M. Gazi (2015). Two-stage batch sorber design and optimization of biosorption conditions by Taguchi methodology for the removal of acid red 25 onto magnetic biomass. Korean Journal of Chemical Engineering, **32**(9), 1864-1878.

Raval, N. P., P. U. Shah and N. K. Shah (2016). Adsorptive amputation of hazardous azo dye Congo red from wastewater: a critical review. Environmental Science and Pollution Research, **23**(15), 14810-14853.

Roginsky, S. and Y. B. Zeldovich (1934). The catalytic oxidation of carbon monoxide on manganese dioxide. Acta Phys. Chem. USSR, **1**, 554.

Roosta, M., M. Ghaedi and F. Yousefi (2015). Optimization of the combined ultrasonic assisted/adsorption method for the removal of malachite green by zinc sulfide nanoparticles loaded on activated carbon: experimental design. RSC Advances, **5**(121), 100129-100141.

Sadaf, S., H. N. Bhatti, S. Nausheen and M. Amin (2015). Application of a novel lignocellulosic biomaterial for the removal of Direct Yellow 50 dye from aqueous solution: Batch and column study. Journal of the Taiwan Institute of Chemical Engineers, **47**, 160-170.

Shiau, C. Y. and C. C. Pan (2005). Adsorption of Basic Dyes from Aqueous Solution by Various Adsorbents. Separation Science and Technology, **39**(8), 1733-1750.

572 Tahir, N., H. N. Bhatti, M. Iqbal and S. Noreen (2017). Biopolymers composites with peanut hull
573 waste biomass and application for Crystal Violet adsorption. International Journal of
574 Biological Macromolecules, **94 Part A**, 210-220.

575 Tran, H. N., F.-C. Huang, C.-K. Lee and H.-P. Chao (2017a). Activated carbon derived from
576 spherical hydrochar functionalized with Triethylenetetramine: synthesis,
577 characterizations, and adsorption application. Green Processing and Synthesis. DOI:
578 10.1515/gps-2016-0178.

579 Tran, H. N., Y.-F. Wang, S.-J. You and H.-P. Chao (2017b). Insights into the mechanism of
580 cationic dye adsorption on activated charcoal: the importance of π-π interactions.
581 Process Safety and Environmental Protection, **17**, 168–180.

582 Tran, H. N., Y.-F. Wang, S.-J. You and H.-P. Chao (2017c). Sustainable Biochar Derived from
583 Agricultural Waste for Removal of Methylene Green 5 from Aqueous Solution:
584 Adsorption Kinetic, Isotherm, Thermodynamic, and Mechanism Analysis.

585 Tran, H. N., S.-J. You, H.-B. Ahmad and H.-P. Chao (2017d). Mistakes and inconsistencies
586 regarding adsorption of contaminants from aqueous solutions: A critical review. Water
587 Research. DOI: DOI: 10.1016/j.watres.2017.04.014.

588 Tran, H. N., S.-J. You and H.-P. Chao (2016a). Effect of pyrolysis temperatures and times on the
589 adsorption of cadmium onto orange peel derived biochar. Waste Management &
590 Research, **34**(2), 129-138.

591 Tran, H. N., S.-J. You and H.-P. Chao (2016b). Thermodynamic parameters of cadmium
592 adsorption onto orange peel calculated from various methods: A comparison study.
593 Journal of Environmental Chemical Engineering, **4**(3), 2671-2682.

594 Tran, H. N., S.-J. You and H.-P. Chao (2017e). Activated Carbons from Golden Shower upon
595 Different Chemical Activation Methods: Synthesis and Characterizations. Adsorption
596 Science & Technology. DOI: 10.1177/0263617416684837.

597 Tran, H. N., S.-J. You and H.-P. Chao (2017f). Fast and efficient adsorption of methylene green 5
598 on activated carbon prepared from new chemical activation method. Journal of
599 Environmental Management, **188**, 322-336.

600 Tran, H. N., S.-J. You and H.-P. Chao (2017g). Insight into adsorption mechanism of cationic dye
601 onto agricultural residues-derived hyrochars: negligible role of π-π interaction. Korean
602 Journal of Chemical Engineering. DOI: 10.1007/s11814-017-0056-7.

603 Wang, H., X. Yuan, Z. Wu, L. Wang, X. Peng, L. Leng and G. Zeng (2014). Removal of Basic
604 Dye from Aqueous Solution using Cinnamomum camphora Sawdust: Kinetics,
605 Isotherms, Thermodynamics, and Mass-Transfer Processes. Separation Science and
606 Technology, **49**(17), 2689-2699.

Weber, W. J. and J. C. Morris (1963). Kinetics of adsorption on carbon from solution. Journal of the Sanitary Engineering Division, **89**(2), 31-60.

Witek-Krowiak, A. (2013). Biosorption of malachite green from aqueous solutions by pine sawdust: equilibrium, kinetics and the effect of process parameters. Desalination and Water Treatment, **51**(16-18), 3284-3294.

Xing, B., W. B. McGill, M. J. Dudas, Y. Maham and L. Hepler (1994). Sorption of phenol by selected biopolymers: isotherms, energetics, and polarity. Environmental Science & Technology, **28**(3), 466-473.

Yang, H., R. Yan, H. Chen, D. H. Lee and C. Zheng (2007). Characteristics of hemicellulose, cellulose and lignin pyrolysis. Fuel, **86**(12–13), 1781-1788.

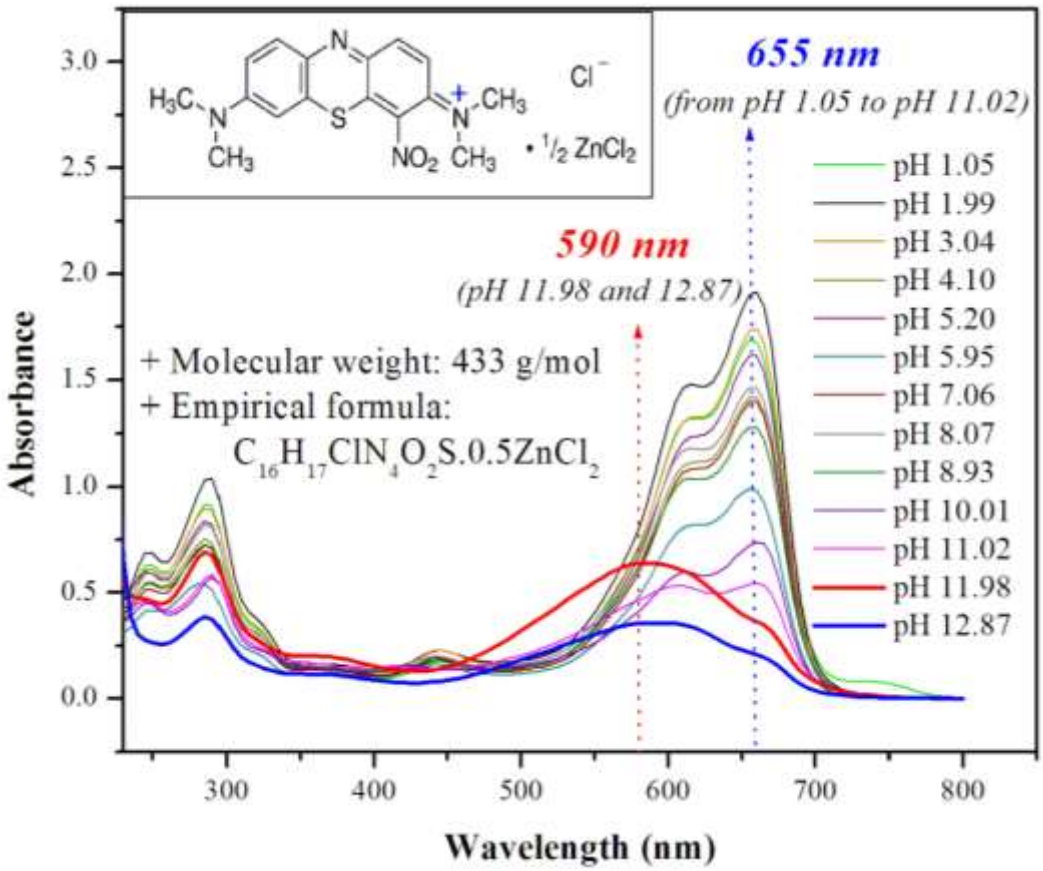

Figure 1. Effect of the pH of the MG5 solution on the λ_{max} value (Data published in our recent work; Tran et al., 2017f)

619

620

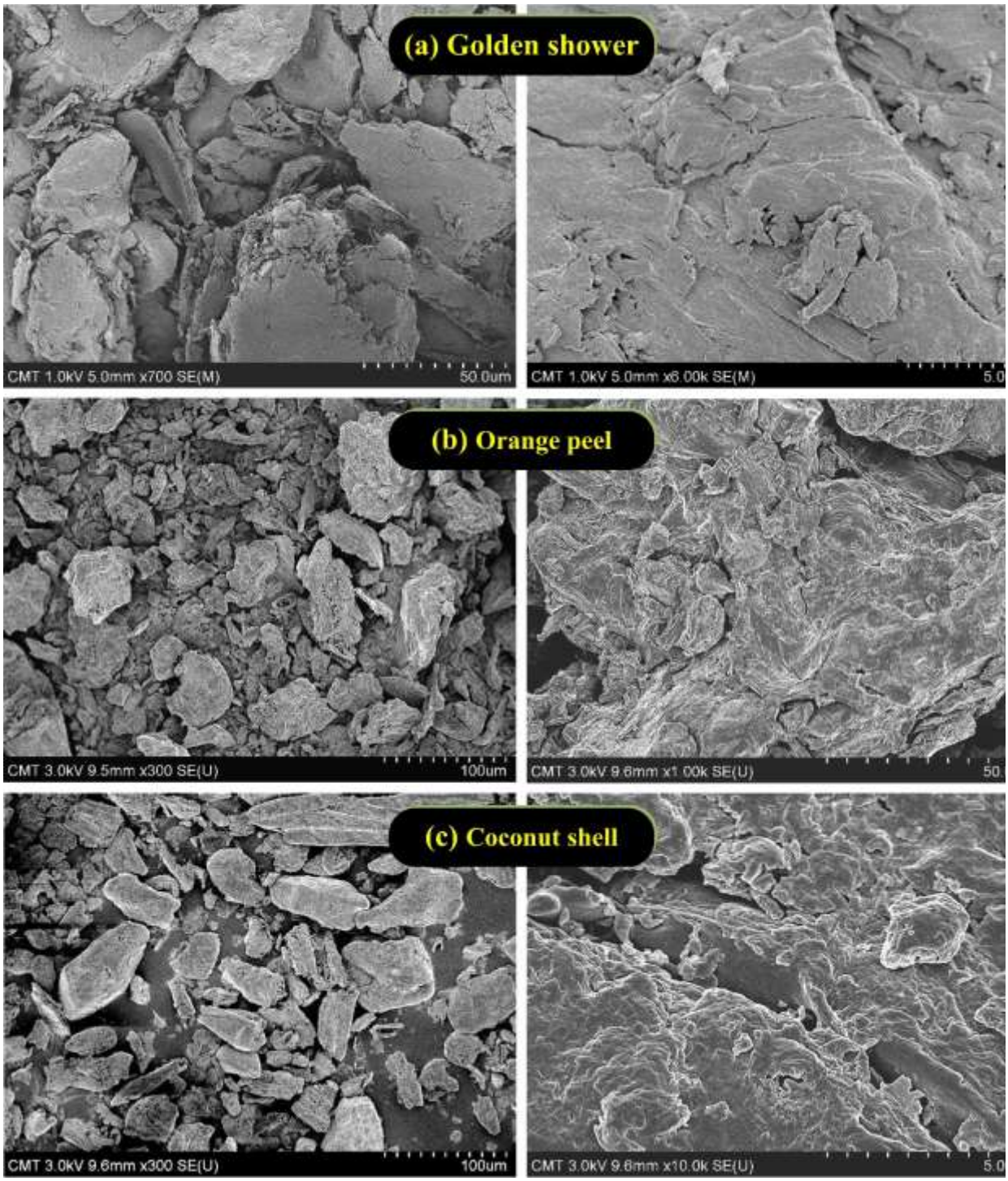

621

622 Figure 2. SEM images of the pristine biosorbent samples

623

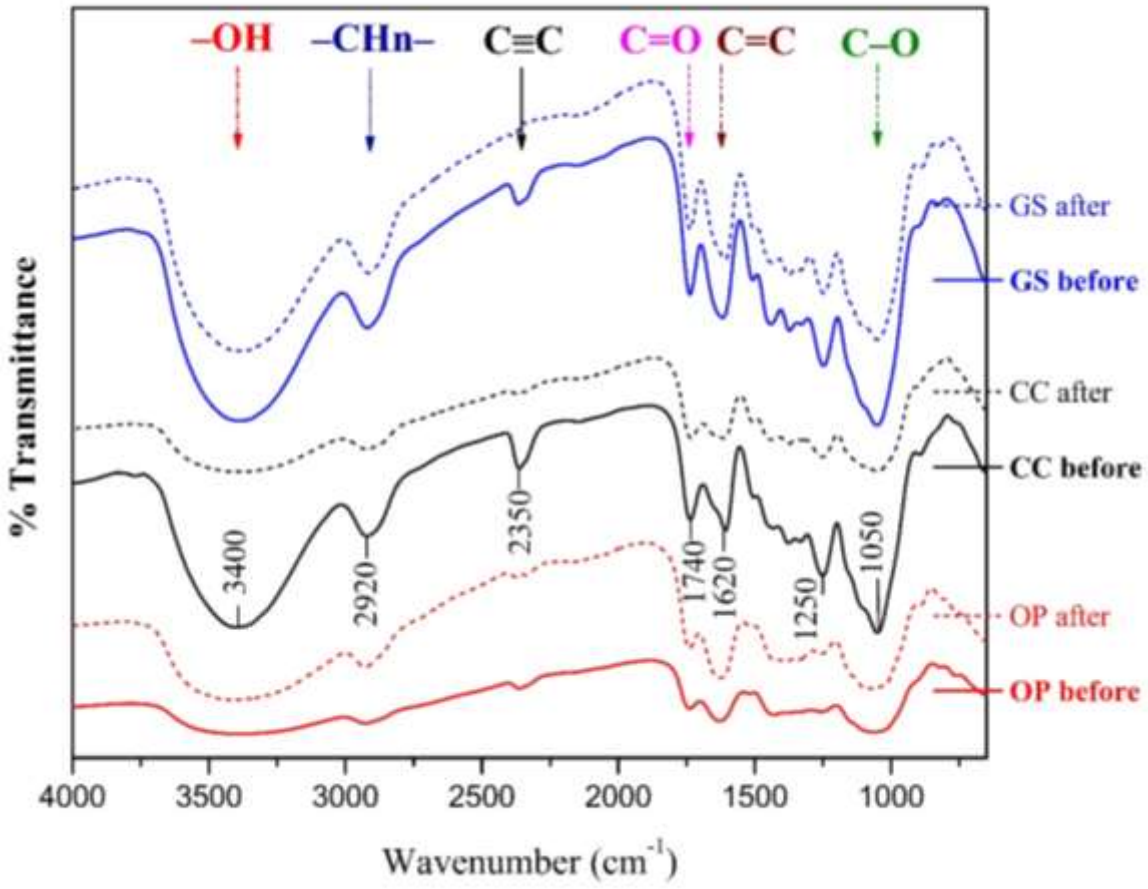

624

625 **Figure 3.** FT-IR spectra of the biosorbents before and after MG5 adsorption

626 (without baseline correction)

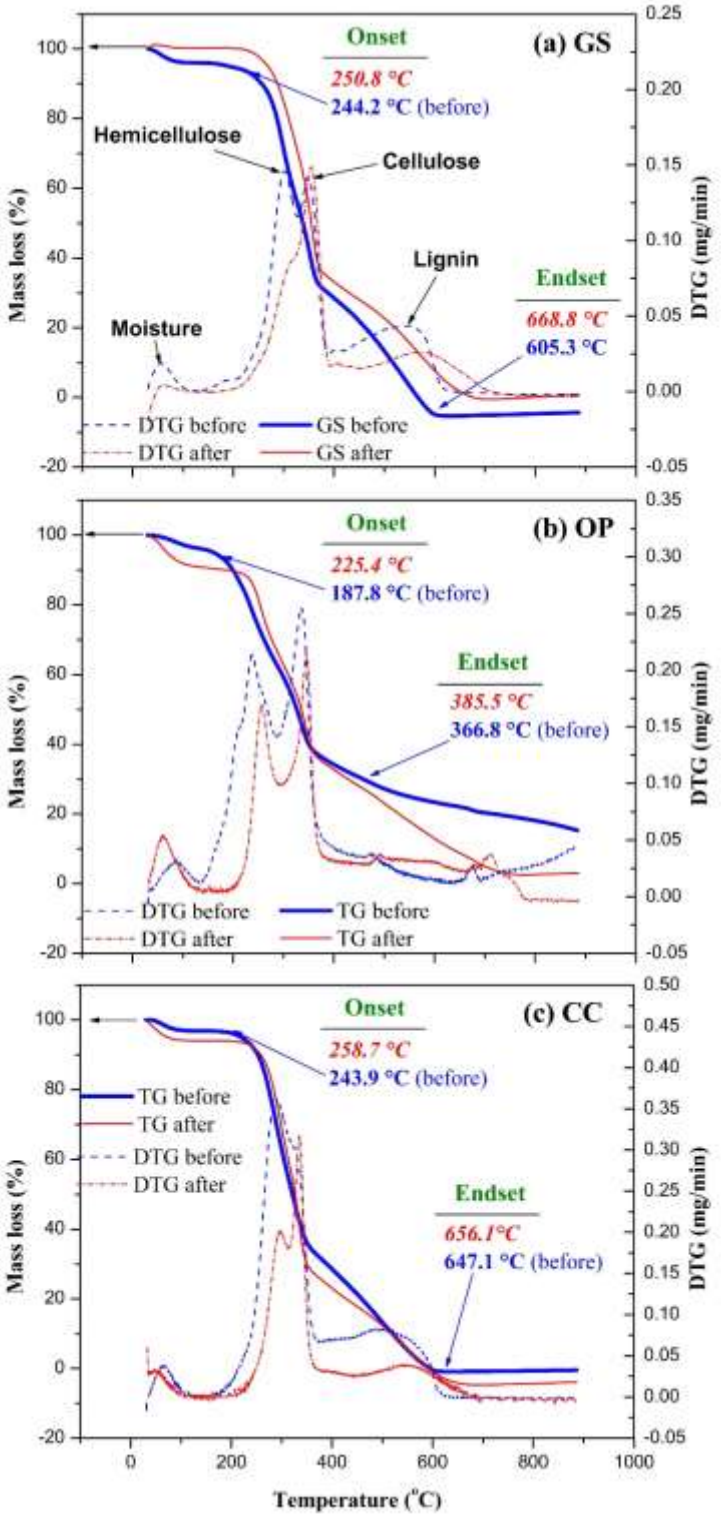

627

628 **Figure 4.** TGA of the biosorbents before and after MG5 adsorption

629

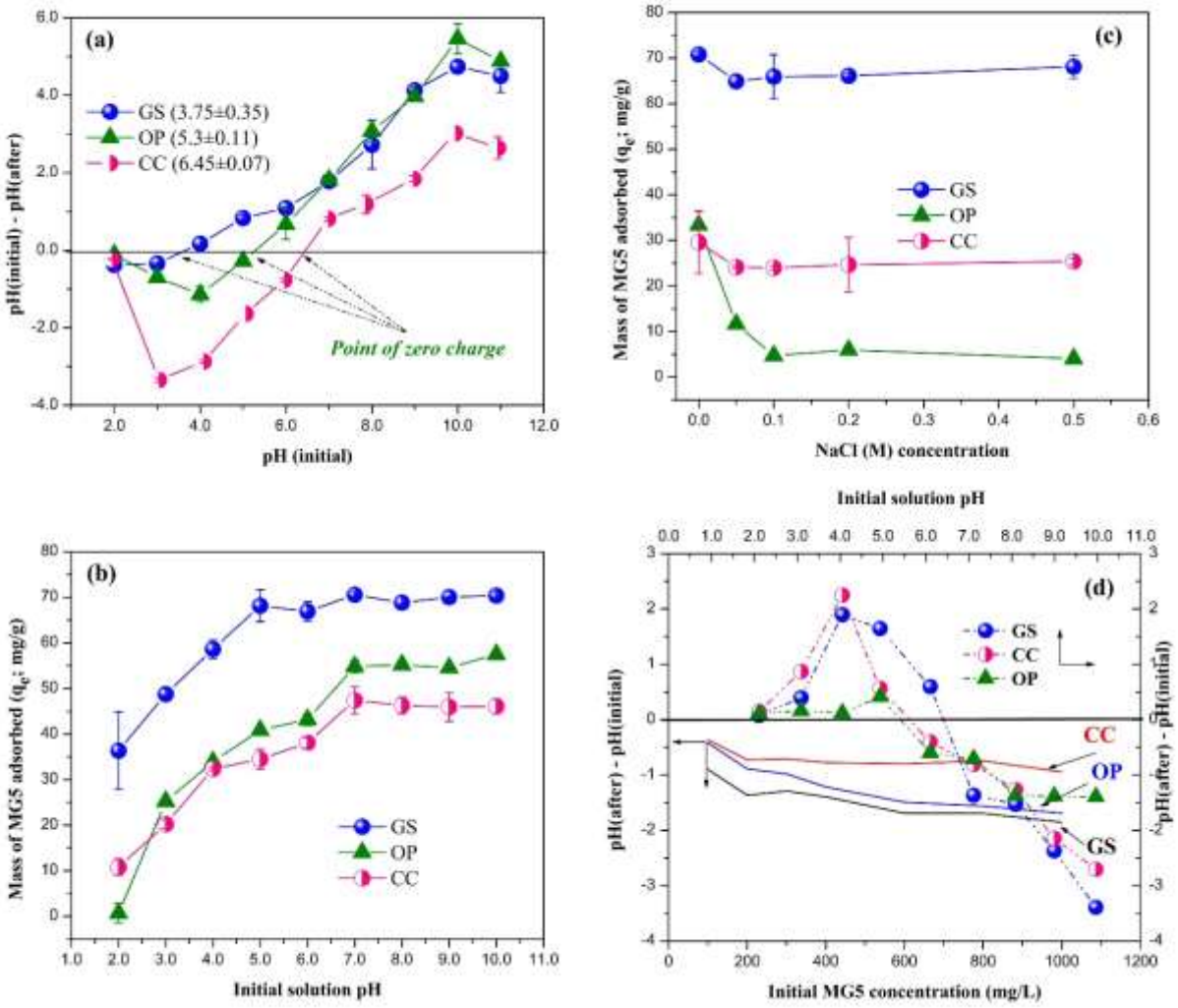

Figure 5. (a) The PZC values of the biosorbents, (b) the dependence of the adsorption capacity on the pH, (c) the effect of the ionic strength on the adsorption capacity, and (d) the pH values after adsorption

(Experimental conditions: t = 24 h, C_0 = 300 mg/L, m/V = 4.0 g/L; 0 M NaCl for the experiments of the dependence of the adsorption capacity on the pH and initial solution pH 7.0 for the experiments of the effect of the ionic strength).

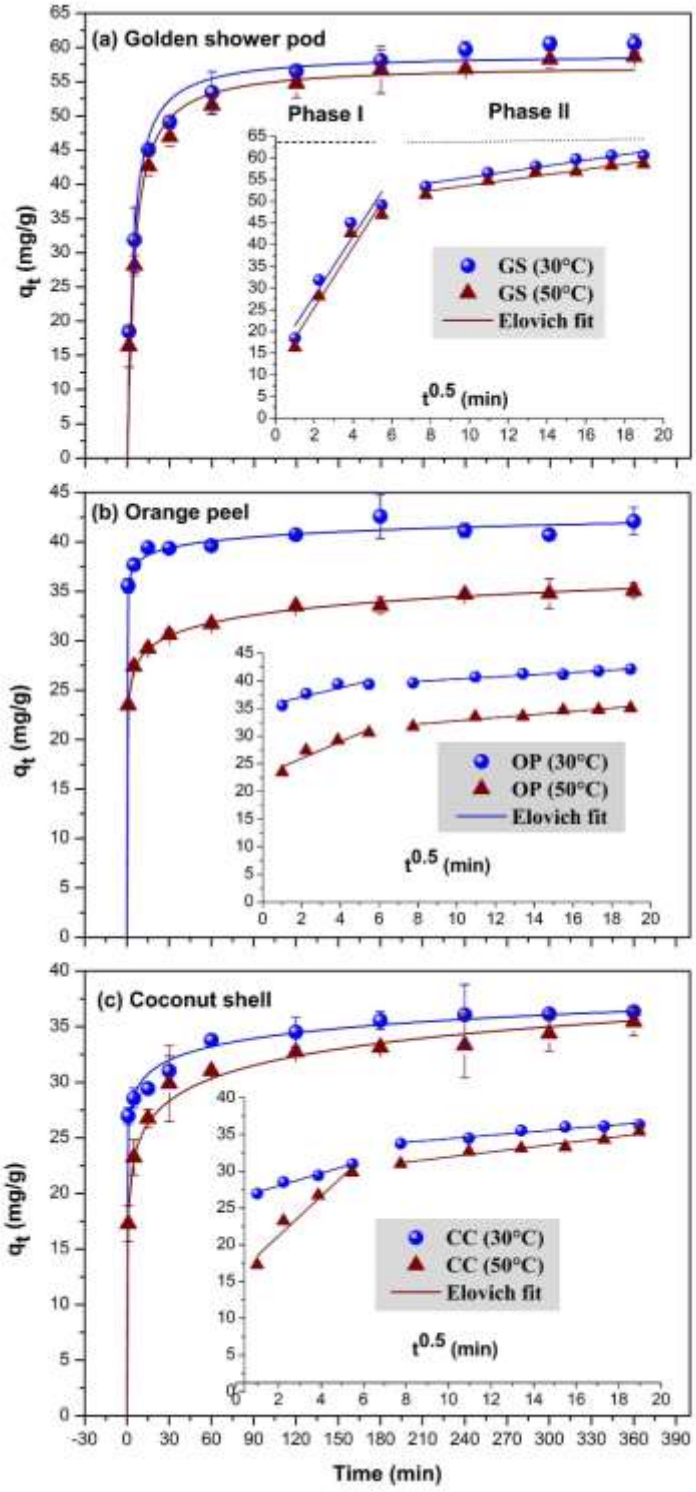

638 **Figure 6.** MG5 adsorption kinetics at different temperatures and intra-particle
639 diffusion plots for MG5 adsorption (figures inside)

640 (Experimental conditions: pH 7.0, 0 M NaCl, m/V = 4.0 g/L, and C_0 = 330 mg/L)

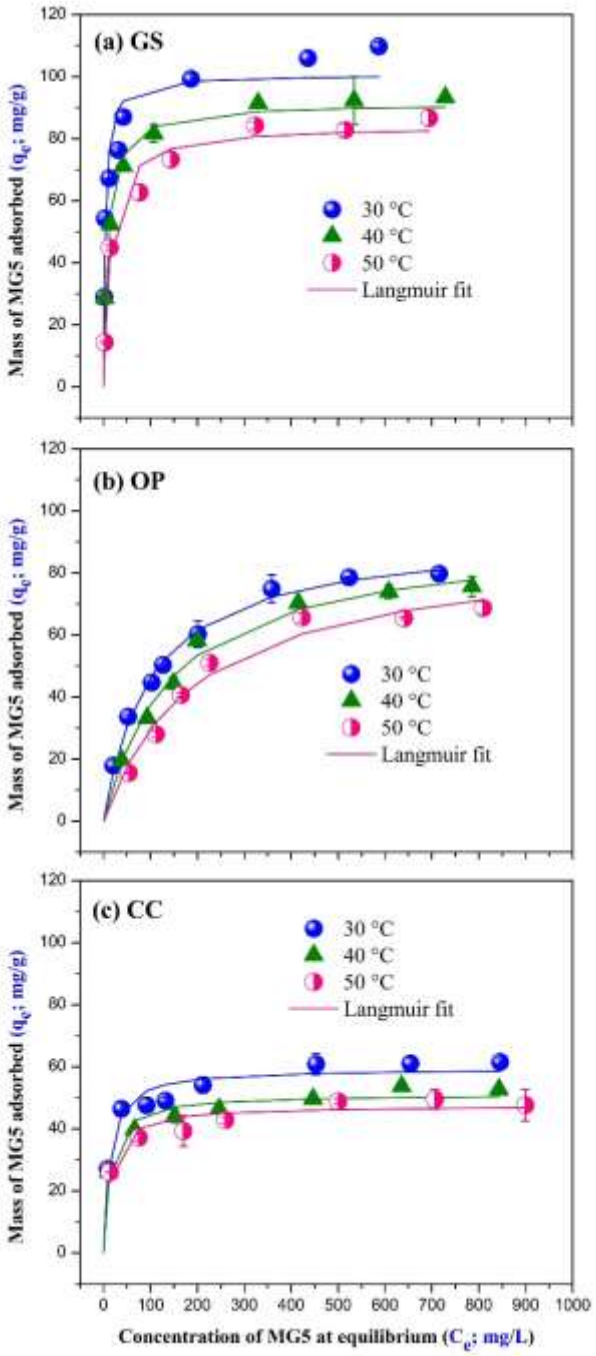

Figure 7. MG5 adsorption isotherms at different temperatures (Experimental conditions: pH 7.0, 0 M NaCl, m/V = 4.0 g/L, t = 24 h, and C_o = 100–1,000 mg/L)

645

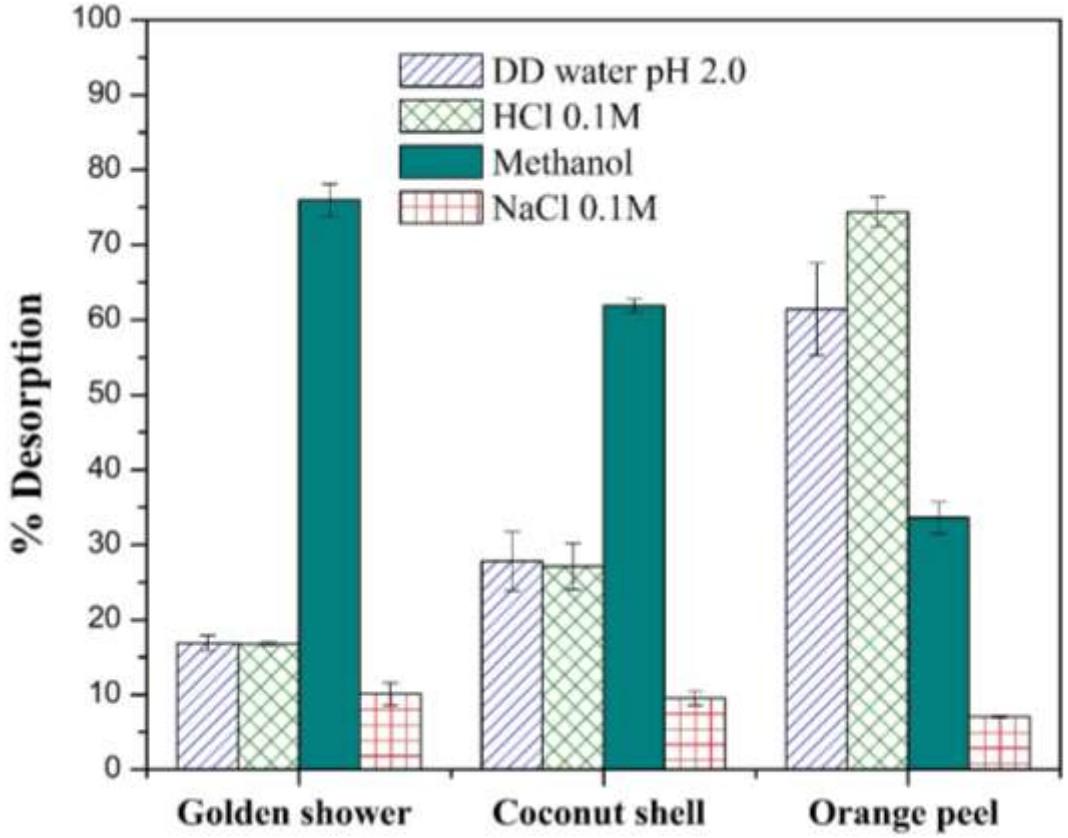

646 **Figure 8.** Percentage of MG5 desorbed using various desorbing agents

647

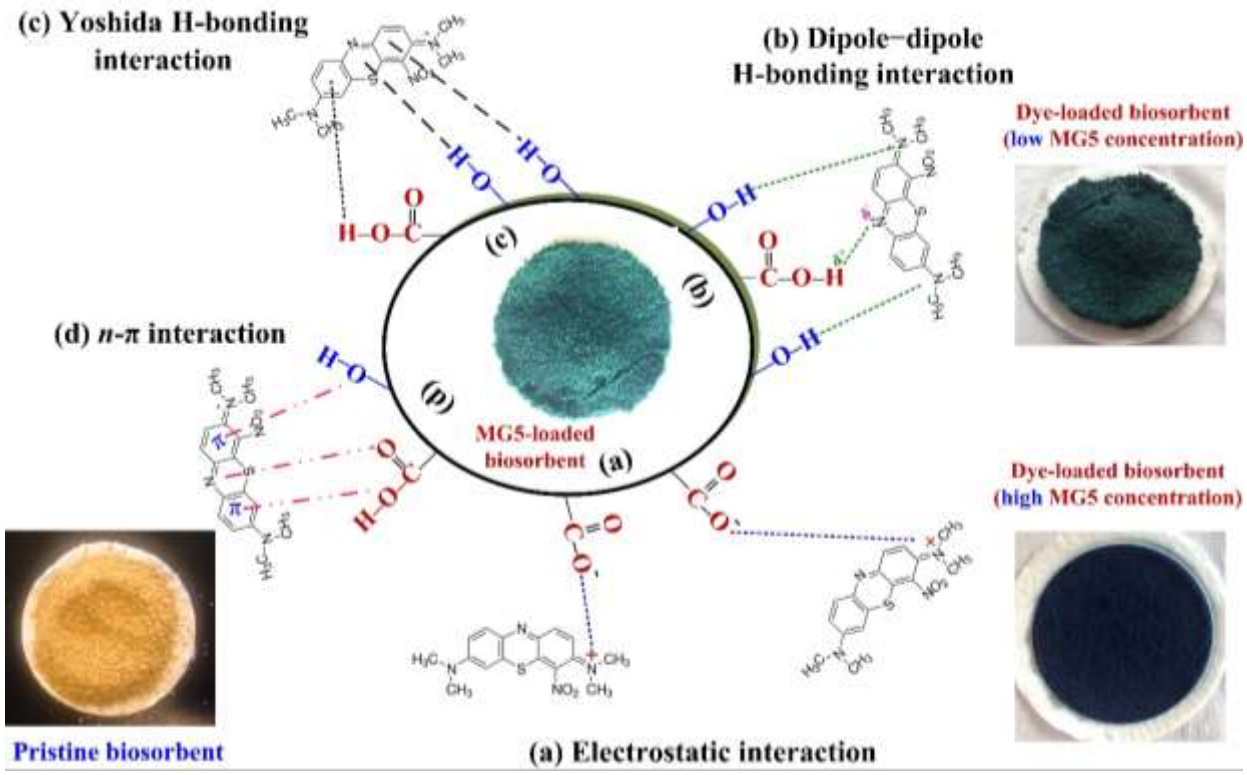

Figure 9. Proposed MG5-adsorption mechanisms for different biosorbents

Table 1. Basic characteristics of the pristine biosorbent samples

	Unit	GS	CC	OP
1. Textural properties				
S_{BET}	m^2/g	5.727	3.167	2.086
$S_{Langmuir}$	m^2/g	16.78	8.093	7.185
$S_{External}$	m^2/g	14.54	6.367	4.339
$V_{total} \times 10^{-3}$	cm^3/g	9.962	4.135	4.237
2. Physicochemical properties				
Hardness	%	49.1±2.01	58.5±2.51	39.7±1.15
Bulk density	g/cm^3	0.66±0.02	0.65±0.20	0.61±0.05
$pH_{1:20}$	–	5.43±0.33	6.5±0.25	4.69±0.18
3. Ultimate analysis				
C	wt%	53.39	55.50	54.34
H	wt%	6.14	6.273	5.91
N	wt%	0.84	0.44	1.14
O[a]	wt%	39.63	37.79	38.61
4. Proximate analysis				
Moisture	wt%	5.80±0.28	8.09±1.59	8.54±1.98
Total ash	wt%	1.17±0.30	1.67±0.15	3.49±0.99
Volatile	wt%	76.2±0.53	73.0±3.34	74.3±2.95
Fixed carbon[a]	wt%	16.8±0.78	17.2±1.91	13.6±2.18
5. Boehm titration results				
Total acidic groups	mmol/g	8.74±0.21	4.21±0.25	6.90±0.38
+ Phenolic	mmol/g	0.37±0.38	2.15±0.95	1.97±0.18
+ Lactonic	mmol/g	1.75±0.21	0.96±0.15	0.85±0.49
+ Carboxylic	mmol/g	6.16±0.14	1.10±0.25	4.07±0.66
Total basic groups	mmol/g	0.12±0.30	2.25±0.55	2.14±0.63

[a]Calculated by difference; means ± standard deviation; $pH_{1:20}$ means approximately 1.0 g adsorbent per 20 mL of distilled deionized water (4h of contact time); data for GS published in our previous study (Tran et al., 2017e).

660 **Table 2.** FTIR spectral characteristics (cm^{-1}) of the biosorbents before and after MG5 adsorption

661

Samples	Functional groups			
	O–H	C=C	C=O	C–O
Pristine GS	3389	1738	1678	1052
MG5-loaded GS	3390	1736	1608	1050
Pristine CC	3392	1734	1613	1050
MG5-loaded CC	3395	1737	1606	1050
Pristine OP	3393	1739	1630	1065
MG5-loaded OP	3397	1739	1625	1073

662

Table 3. T_{max} values and mass loss percentages of the main components of the biosorbents before and after the adsorption of MG5

DTG peak	T_{max} (°C)/mass loss (%)						Definition
	Before MG5 adsorption			After MG5 adsorption			
	GS	CC	OP	GS	CC	OP	
1	54/1.39	61/1.02	87/2.01	57/0.21	53/3.06	61/3.66	Moisture
2	299/26.8	289/28.7	237/19.5	320/25.8	299/27.0	256/17.8	Hemicellulose
3	351/30.1	327/23.5	333/32.4	356/26.0	335/28.2	346/34.6	Cellulose
4	–	–	490/18.1	–	–	492/20.1	CaO
5	548/37.9	498/33.2	700/27.9	583/37.8	540/34.7	711/23.4	Lignin

Table 4. Corresponding adsorption kinetic parameters for MG5 adsorption by GS, CC, and OP

	GS		OP		CC	
	30 °C	**50 °C**	**30 °C**	**50 °C**	**30 °C**	**50 °C**
$q_{e,exp}$	60.30	56.89	41.58	34.54	35.03	32.07
Pseudo-first-order model						
$q_{e,cal}$	59.39	54.76	40.30	32.32	33.49	31.45
k_1	0.162	0.131	2.822	1.283	1.632	0.612
R^2	0.844	0.874	0.540	0.488	0.258	0.577
χ^2	30.81	25.94	5.105	7.336	9.247	13.85
Pseudo-second-order model						
$q_{e,cal}$	59.02	57.45	40.69	33.03	34.08	32.72
k_2 ($\times 10^{-3}$)	4.412	3.695	151.7	60.66	85.64	23.66
R^2	0.953	0.963	0.653	0.716	0.475	0.833
χ^2	9.165	7.640	1.514	4.062	6.551	5.468
Elovich model						
α ($\times 10^3$)	0.154	0.100	2108	456.6	4.065	1.682
β	0.141	0.138	0.982	0.518	0.564	0.345
R^2	0.961	0.957	0.967	0.994	0.955	0.976
χ^2	7.723	8.681	0.133	0.089	0.556	0.776
Intra-particle diffusion model						
K_{ip}	1.863	1.897	0.285	0.536	0.519	0.779
C	31.39	28.79	37.14	26.25	27.84	22.19
R^2	0.741	0.739	0.833	0.847	0.911	0.784
χ^2	11.85	13.07	0.161	0.687	0.307	2.508
Activation energy						
$Ea(k_1)$	-8.64		-32.07		-39.90	
$Ea(k_2)$	-7.22		-37.29		-52.33	
$Ea(\alpha)$	-17.45		-62.23		-35.23	
$Ea(k_{ip})$	-3.52		-14.12		-9.23	

Note: *the units of kinetic parameters are q_e (mg/g), β (mg/g), k_1 (1/min), k_2 (g/mg×min), k_{ip} (mg/g×min), α (g/mg×min), Ea (kJ/mol). The kinetic parameters were determined by non-linear method, expected for the intra-particle diffusion model.*

672 **Table 5.** Relative adsorption isotherm parameters for MG5 adsorption

	Units	Golden shower pod (GS)			Orange peel (OP)			Coconut shell (CC)		
		30 °C	40 °C	50 °C	30 °C	40 °C	50 °C	30 °C	40 °C	50 °C
Langmuir parameters										
Q^o_{max}	mg/g	105.6	91.35	84.16	92.35	91.96	88.88	59.47	51.1	47.5
K_L	L/mg	0.132	0.106	0.072	0.010	0.007	0.005	0.079	0.076	0.071
R^2	–	0.966	0.973	0.971	0.993	0.991	0.969	0.916	0.915	0.824
χ^2	–	4.67	3.88	2.17	0.71	0.9	1.95	1.66	1.10	1.63
Freundlich parameters										
K_F	$(mg/g)/(mg/L)^n$	40.4	34.8	23.4	9.05	6.89	4.56	22.1	20.1	19.3
n	–	0.164	0.159	0.210	0.344	0.371	0.417	0.160	0.149	0.142
R^2	–	0.915	0.881	0.925	0.956	0.967	0.905	0.951	0.960	0.954
χ^2	–	12.3	6.77	11.5	3.99	5.05	10.7	1.24	0.57	0.95
Dubinin-Radushkevich parameters										
Q_{DR}	mg/g	87.4	81.0	78.5	72.7	73.6	67.5	55.0	48.0	44.4
K_{DR}	mol^2/kJ^2	0.74	1.76	15.36	498.21	1191.70	1593.91	10.96	13.13	13.67
E	kJ/mol	0.822	0.532	0.180	0.032	0.020	0.018	0.214	0.195	0.191
R^2	–	0.770	0.703	0.867	0.783	0.845	0.907	0.748	0.764	0.702
Separation factor										
R_L	$\times 10^{-3}$	7.2–60.3	8.6–74.1	13–126	88–508	116–550	155–629	11.4–97	12–101	13–106

673 *Note: the parameters from the selected models were determined using non-linear method.*

674 **Table 6.** Adsorption thermodynamics parameters for MG5 adsorption

T (K)	van't Hoff equation	K_C	ΔG^o (kJ/mol)	ΔH^o (kJ/mol)	ΔS^o (J/mol × K)
Golden shower pod (GS)					
303	y = 2956x+2.07	131900	-29.72	-24.57	17.21
313	R^2 = 0.969	105900	-30.12		
323		72000	-30.05		
Orange peel (OP)					
303	y = 3407x - 2.03	10022	-23.22	-28.33	-18.32
313	R^2 = 0.999	6933	-23.03		
323		5000	-22.88		
Coconut shell (CC)					
303	y = 499x + 9.63	79100	-28.43	-4.151	80.10
313	R^2 = 0.991	75652	-29.25		
323		71423	-30.03		

675

676

677

678

679 **Table 7.** Comparison of the cationic dye maximum capacities (Q^{o}_{max}) of the biosorbents studied
680 here and those of other biosorbents reported in the literature

Biosorbent	Dye	Mw (g/mol)	Q^{o}_{max} (mmol/g)	Reference
Cinnamomum camphora	MG	365	0.424	Wang et al. (2014)
Simarouba glauca	MG	365	0.342	Jeyagowri and Yamuna (2016)
Orange peel	BB41	483	0.326	Contreras et al. (2012)
Chitosan aniline composite with PH	CV	408	0.257	Tahir et al. (2017)
Starch composite with PH	CV	408	0.248	Tahir et al. (2017)
Golden shower	**MG**	**433**	**0.244**	**This study**
Chitosan pyrrole composite with PH	CV	408	0.229	Tahir et al. (2017)
Polyaniline composite with PH	CV	408	0.221	Tahir et al. (2017)
Polypyrrole composite with PH	CV	408	0.218	Tahir et al. (2017)
Orange peel	**MG5**	**433**	**0.213**	**This study**
Pine sawdust	MG	365	0.196	Witek-Krowiak (2013)
Coconut shell	**MG5**	**433**	**0.137**	**This study**
Brewer's spent grains	BB41	483	0.067	Contreras et al. (2012)
Banana peel	MB	320	0.065	Annadurai et al. (2002)
Orange peel	MB	320	0.058	Annadurai et al. (2002)
Banana peel	MV	256	0.048	Annadurai et al. (2002)
Orange peel	MV	256	0.045	Annadurai et al. (2002)
Banana peel	RB	479	0.043	Annadurai et al. (2002)
Orange peel	RB	479	0.030	Annadurai et al. (2002)

Note: *MG5 (methylene green 5); MG (Malachite green); MB (Methylene blue); MV (Methyl violet); RB (Rhodamine B); BB41 (Basic Blue 41); CV (Crystal Violet*); *and PH (peanut hull)*

685 **Table 8.** Comparison of the maximum capacities (Q^o_{max}) of MG5 adsorption by the biosorbents
686 studied here and those of other adsorbents reported in the literature

Adsorbent	S_{BET} (m^2/g)	pH	T (°C)	Q^o_{max} (mg/g)	Reference
Biosorbent					
Golden shower	5.727	7.0	30	**106**	***This study***
Coconut shell	3.167	7.0	30	**59.5**	***This study***
Orange peel	2.086	7.0	30	**92.4**	***This study***
Hydrochar					
Golden shower	14.7	7.0	30	59.6	Tran et al. (2017g)
Coconut shell	6.65	7.0	30	32.7	Tran et al. (2017g)
Orange peel	6.99	7.0	30	15.6	Tran et al. (2017g)
Commercial glucose	7.08	5.0	25	13.9	Tran et al. 2017a)
Biochar					
Golden shower	604	7.0	30	45.5	Tran et al. (2017c)
Coconut shell	536	7.0	30	41.5	Tran et al. (2017c)
Orange peel	565	7.0	30	35.2	Tran et al. (2017c)
Activated carbon					
Golden shower	812–1,413	7.0	30	253–531	Tran et al. (2017f)
Orange peel	1,025	7.0	30	330	Tran et al. (2017f)
Commercial glucose	335	5.0	25	175	Tran et al. (2017a)
Commercial AC	768	5.0	25	178	Huang et al. (2014)
Commercial xylose	1,386	5.0	25	417	Huang et al. (2014)
Commercial sucrose	1,494	5.0	25	299	Huang et al. (2014)
Commercial glucose	1,612	5.0	25	444	Huang et al. (2014)
Norit RB4C	1,026	7.0	30	543	Tran et al. (2017b)
Activated carbon	946	3.0	25	272	Shiau and Pan (2005)
Others					
Ag-NP-AC	NA	7.0	25	167	Ghaedi et al. (2014)
ZnONR-AC	NA	7.0	25	200	Ghaedi et al. 2014)
MCM-41	1,004	4.0	25	137	Lee et al. (2007)
GH-$TETA_{1\%}$	NA	5.0	25	67.6	Tran, et al. (2017a)
$GAC_{1\%}$	233	5.0	25	101	Tran, et al. (2017a)
Montmorillonite	165	3.0	25	128	Shiau and Pan (2005)
Activated clay	278	3.0	25	271	Shiau and Pan (2005)
Titania nanotube	292	4.0	25	292	Lin et al. (2010)

687

688